Evidence for fractional crystallization of wadsleyite and ringwoodite from olivine melts in chondrules entrained in shock-melt veins

Masaaki Miyahara*†, Ahmed El Goresy‡, Eiji Ohtani*, Toshiro Nagase§, Masahiko Nishijima¶, Zahra Vashaei¶, Tristan Ferroir∥, Philippe Gillet∥, Leonid Dubrovinsky‡, and Alexandre Simionovici**

*Institute of Mineralogy, Petrology, and Economic Geology, Graduate School of Science, Tohoku University, Sendai 980-8578, Japan; ‡Bayerisches Geoinstitut, Universität Bayreuth, D-95440, Bayreuth, Germany; §Tohoku University Museum, Tohoku University, Sendai 980-8578, Japan; ¶Institute for Materials Research, Tohoku University, Sendai 980-8577, Japan; ∥Laboratoire des Sciences de la Terre, Université de Lyon, Ecole Normale Supérieure de Lyon, Université Claude Bernard Lyon 1, Centre National de la Recherche Scientifique 46 Allée d'Italie, 69364 Lyon Cedex 07, France; and **Observatoire des Sciences, Laboratoire Géophysique Interne et Tectonophysique, Université de Grenoble, 38041 Grenoble Cedex 9, France

Peace River is one of the few shocked members of the L-chondrites clan that contains both high-pressure polymorphs of olivine, ringwoodite and wadsleyite, in diverse textures and settings in fragments entrained in shock-melt veins. Among these settings are complete olivine porphyritic chondrules. We encountered few squeezed and flattened olivine porphyritic chondrules entrained in shock-melt veins of this meteorite with novel textures and composition. The former chemically unzoned (Fa_{24-26}) olivine porphyritic crystals are heavily flattened and display a concentric intergrowth with Mg-rich wadsleyite of a very narrow compositional range (Fa_6–Fa_{10}) in the core. Wadsleyite core is surrounded by a Mg-poor and chemically stark zoned ringwoodite (Fa_{28}–Fa_{38}) belt. The wadsleyite–ringwoodite interface denotes a compositional gap of up to 32 mol % fayalite. A transmission electron microscopy study of focused ion beam slices in both regions indicates that the wadsleyite core and ringwoodite belt consist of granoblastic-like intergrowth of polygonal crystallites of both ringwoodite and wadsleyite, with wadsleyite crystallites dominating in the core and ringwoodite crystallites dominating in the belt. Texture and compositions of both high-pressure polymorphs are strongly suggestive of formation by a fractional crystallization of the olivine melt of a narrow composition (Fa_{24-26}), starting with Mg-rich wadsleyite followed by the Mg-poor ringwoodite from a shock-induced melt of olivine composition (Fa_{24-26}). Our findings could erase the possibility of the resulting unrealistic time scales of the high-pressure regime reported recently from other shocked L-6 chondrites.

focused ion beam | transmission electron microscopy | shocked chondrite | high-pressure mineral

Many highly equilibrated L- and H-chondritic meteorites display intense deformation of their mineral constituents, olivine, orthopyroxene, and plagioclase feldspars, inferred to have been produced by hypervelocity collisions of their parental asteroids with other interplanetary objects. They also contain millimeter-sized shock-melt veins interpreted to have resulted from friction along cracks or concentration of shear in glide bands as a result of the deviatoric component rather than from pressure heterogeneities during the dynamic events. The melt veins contain an inventory of high-pressure polymorphs of the major chondritic minerals olivine, orthopyroxene, and plagioclase feldspars like ringwoodite, less abundant wadsleyite, majorite, akimotoite, lingunite, and jadeite plus SiO_2 glass. In many chondrites, the matrices of these veins show the liquidus pair majorite-pyrope$_{ss}$ plus magnesiowüstite and FeNi metal blebs with eutectic-like intergrowth with FeS indicating crystallization from a melt of bulk chondritic composition at high pressures (≈ 20–23 GPa) and temperatures (2,000–2,300°C) (1). The oli-

vine–ringwoodite and olivine–wadsleyite inversions in these veins were extensively investigated due to their relevance to mechanisms in Earth's transition zone and the lower mantle. The shock-induced high-pressure phases in the melt veins may mimic phase-transformation processes active in planetary interiors. In addition to pressure, the influence of other parameters such as thermal stress and grain size of the olivine grains on the nucleation, growth rates, and mechanisms of phase transitions, if coherent or incoherent, were extensively studied in laboratory multianvil experiments (e.g., refs. 2 and 3) and are critical in deducing the duration of the shock events in asteroids. Many ringwoodite and majorite grains encountered in shock-melt veins are polycrystalline with triple junctions and have identical chemical compositions with their parental low-pressure phases (e.g., refs. 1, 4, and 5). It is generally accepted that these ringwoodite and majorite grains were formed by direct solid-state phase-transformation mechanisms. Wadsleyite of similar composition of coexisting ringwoodite first encountered in melt veins in Peace River chondrite was interpreted to have formed by solid-state back transformation from ringwoodite (4, 6, 7). Large olivine grains intersected by bands of ringwoodite whose chemical compositions are different from the parental olivine were also encountered in shock-melt veins or adjacent zones in the Sixiangkou L6 chondrite and were interpreted to have formed by diffusion-controlled intracrystalline solid-state nucleation and growth along shock-induced fractures (8–10). This assumption, with one exception (11), resulted in unrealistically long time scales between several tens of seconds (8–10) and up to 500 s (10, 12) for the duration of the high-pressure regime. However, only Ohtani *et al.* (12) cautiously cast doubt on the relevance of these estimated long time scales.

We have encountered in the Peace River chondrite few squeezed and flattened olivine-bearing chondrules whose former olivines now consist of concentric intergrowths of Mg-depleted ringwoodite and Mg-rich wadsleyite and large olivine grains with thick ringwoodite veins or bands whose chemical compositions have olivine stoichiometry along fractures. The first setting is a finding whose study, as we show in this article, led to a better understanding of the multistage mechanisms involved and, consequently, erases the time scale discrepancy. We confine our interest in this article to the intergrowth in the

olivine chondrules. Results of the ringwoodite thick veins in large olivine grains will be reported in detail elsewhere (T.F., M.M., A.E.G., E.O., T.N., M.N., Z.V., P.G., L.D., and A.S., unpublished work).

The Peace River L6 chondrite is one of the few shocked L6 chondrites that contains high-pressure polymorphs of olivine, ringwoodite, and wadsleyite in the shock-melt veins (13, 14). Price *et al.* (13, 14) reported that the wadsleyite they studied in Peace River is similar in composition to the parental olivine and coexisting ringwoodite. Hence, they conclude that it was produced by back transformation of ringwoodite to wadsleyite in the decompression stage. Study of the textural relations and chemical compositions of the three polymorphs in the different settings in Peace River may open a new venue to realistically scrutinize the mechanisms of their formation and ultimately clarify the time scale conundrum.

In this article, we present results of comprehensive fine-scale textural, chemical, laser microRaman, and surgical transmission electron microscopy (TEM) investigations of focused ion beam (FIB) cuts of the assemblage in an entrained olivine chondrule containing ringwoodite and wadsleyite.

Results

The large olivine grains entrained in the shock-melt veins are pervasively intersected by thick bright ringwoodite veins (up to 12 μm in thickness) with dark wadsleyite patches on both interfaces to parental olivine. In contrast, the original olivine phencrysts in the chondrules are severely flattened and depict a concentric texture with Mg-rich wadsleyite filling the interiors of the individual original olivine pophyritic crystals circularly surrounded by Fe-rich ringwoodite bands (Fig. 1a). Raman mapping confirmed the circular arrangements of wadsleyite core and ringwoodite rim (Fig. 1c). Electron microprobe analysis of the individual polymorphs revealed that the wadsleyite core is rich in Mg (Fa$_{12}$), whereas the ringwoodite rim is depleted in Mg (Fa$_{31-36}$).

We selected typical ringwoodite- and wadsleyite-bearing former olivines in the chondrule (dashed line in Fig. 1a) containing wadsleyite cores for a FIB–TEM/scanning TEM (STEM) investigation. Four FIB slices (nos. 1, 2, 3, and 4B) in the ringwoodite–wadsleyite grains were extracted by using a FIB system and studied by TEM/STEM-energy dispersive x-ray spectroscopy (EDS). Bright-field (BF)-TEM images show that the ringwoodite-bearing area consists of a polycrystalline assemblage of ringwoodite and wadsleyite in an intergrowth feigning granoblastic-like texture (Fig. 2b). Both ringwoodite and wadsleyite are polygonal equigranular, with a diameter between 0.5 and 1.5 μm. The interface boundary between the crystallites is usually straight, with no evidence of chemical concentration profiles that might be suggestive of diffusion. Ringwoodite crystallites appear to be full of lineaments (Fig. 2c); because of the dense stacking faults compared with wadsleyite, the latter depicts clear crystallites. No ringwoodite–wadsleyite lamellar intergrowth was encountered in this area so far. We could not observe any preferred crystallographic orientation relationship between ringwoodite and wadsleyite crystallites. Dendrite-like textures were observed at boundaries between the ringwoodite-bearing region and the Ca-poor pyroxene grain (Fig. 3 a and b). Selected area electron diffraction (SAED) patterns indicate that the dendrite-like parts are amorphous or poorly crystallized (Fig. 3d). Crystallites ($\approx$200 nm) in the core of the dendrites are verified as wadsleyite based on their SAED patterns (Fig. 3c). The boundary between the dendrite–wadsleyite–ringwoodite-bearing region and the adjacent Ca-poor pyroxene is knife sharp, with no evidence of melting, reaction, or mixing with the Ca-poor pyroxene. This region is intersected by veins containing secondary iron oxides between the ringwoodite-bearing grain and Ca-poor pyroxene grain (Fig.

Fig. 1. A flattened chondrule in a shock-melt vein selected for this study. (a) BSE image. Dark-colored patches in the interior of the former olivines in BSE image are Mg-rich wadsleyite. Gray portions are Fe-rich ringwoodite. (b) Scanning ion microscopy (SIM) image (dashed line in a). Nos. 1, 2, 3, and 4B are slices extracted by FIB cuts for this study. The dimension of nos. 1, 2 3, and 4B slices are $\approx$11 × 6 μm, 10 × 7 μm, 9 × 5 μm, and 11 × 7 μm, respectively. (c) The laser Raman spectroscopy mapping of the ringwoodite–wadsleyite assemblage in two adjacent former olivines is now pushed together through flattening of the chondrule (dashed line in a). Pyroxene is displayed as green, ringwoodite as red, and wadsleyite as blue. No trace of olivine was found in this area. Rgt, ringwoodite; Wds, wadsleyite; Jd, jadeite; Cpx, Ca-poor pyroxene; FeNi, iron–nickel alloy; Ak, akimotoite.

3a). A large metal grain in the flattened chondrule (Fig. 1a, white on left side) displays scalloped outlines indicating melting. The former plagioclase (Ab$_{82}$An$_{12}$Or$_6$) (now consisting of jadeite and SiO$_2$ glass) also depicts amoeboid outlines in few grains, but their majority display polygonal outlines (Fig. 1a), thus indicating only localized melting.

The chemical compositions of ringwoodite and wadsleyite were obtained by STEM-EDS (Table 1). There is a distinct difference in chemical compositions between ringwoodite and wadsleyite crystallites (Fig. 2a). Ringwoodite has an average Mg# of 68, whereas wadsleyite has an Mg# of 91 [Mg# = 100 × Mg/(Mg + Fe)] (except for wadsleyite in the core of the dendrite part). Compositional ranges of the coexisting crystallites of both polymorphs are distinct: Wadsleyite compositions are quite narrow (Fa$_6$–Fa$_{12}$), whereas the ringwoodite compositions vary between Fa$_{28}$ and Fa$_{38}$. The compositional gap between the wadsleyite highest in fayalite and the ringwoodite lowest in the same molecule is 32 mole %. The chemical compositions of dendrite-like parts appear to be (Mg, Fe)$_2$SiO$_4$ (Fa$_{26}$), thus identical to the composition of the parental unzoned olivine (Table 1). This article reports these highly contrasting compositions of coexisting high-pressure olivine polymorphs and hints to a distinct formational mechanism other than solid-state phase transformation.
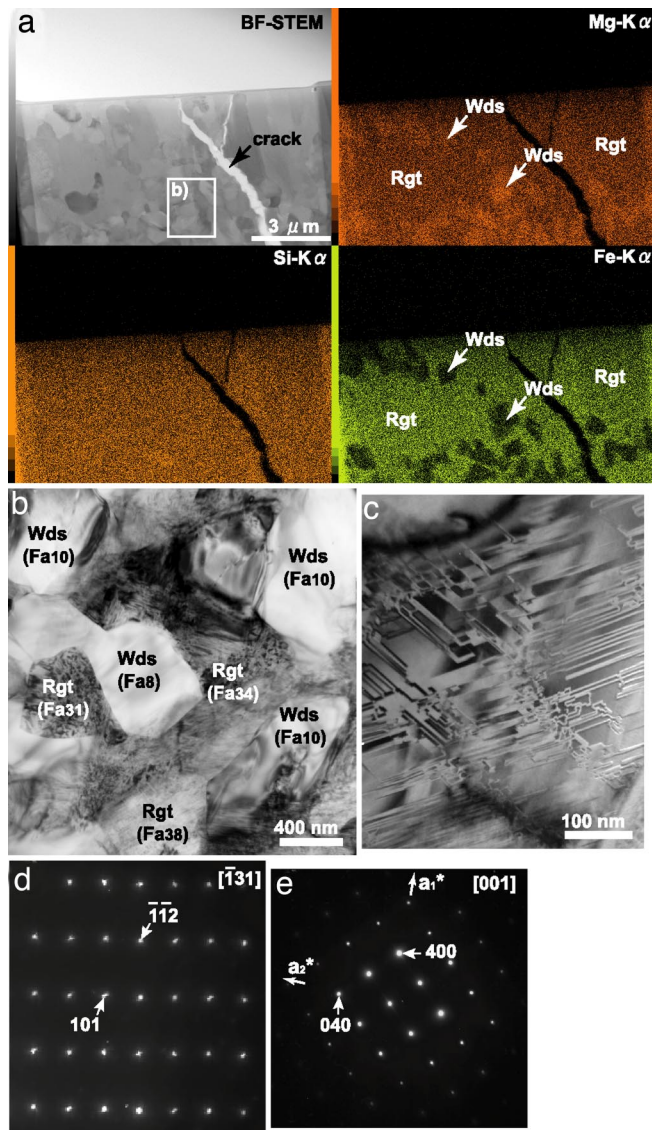
GEOLOGY

Fig. 2. TEM images of no. 1 slice. (*a*) A bright-field (BF)-STEM image and Mg, Si, and Fe elemental mapping images of ringwoodite–wadsleyite assemblage. Elemental mapping images were obtained by using STEM-EDS under BF-STEM image. (*b*) BF-TEM image indicates that ringwoodite and wadsleyite are equigranular. (*c*) High-density stacking faults in ringwoodite. The stacking fault density of ringwoodite is much larger than that of wadsleyite. (*d* and *e*) SAED patterns of wadsleyite and ringwoodite, respectively.

Fig. 3. TEM images of FIB slice no. 3. (*a*) High-angle annular dark field (HAADF) image depicting a wadsleyite–ringwoodite assemblage. HAADF appear to correspond to Z-contrast image. (*b*) BF-TEM image of dendrite-like texture (box in *a*). (*c*) SAED patterns of wadsleyite core part in *b*). (*d*) SAED patterns of a poorly crystallized or amorphous (dendrite-like) part having Fa_{26} compositions in *b*.

Discussion

The matrix portion of a shock-melt vein consists of ringwoodite, wadsleyite, akimotoite, and iron-nickel, metal-troilite, eutectic-like FeNi–FeS spherules. Based on the phase diagram determined by high-pressure melting experiments of the Allende meteorite (15, 16), we may constrain the pressure conditions during a shock event of Peace River L6 chondrite. Considering the coexistence of ringwoodite and wadsleyite, both the deformed chondrule and matrix were subjected to the same pressure of at least 13–18 GPa.

We encountered few characteristic flattened and squeezed chondrules in the shock-melt vein of Peace River L6 chondrite. One of them is depicted in Fig. 1. The deformed chondrule consists of ringwoodite, wadsleyite, former plagioclase (now consisting of jadeite and SiO_2 glass), Ca-poor pyroxene, troilite, and scalloped iron-nickel metal. Fine-grained porphyroblastic-like ringwoodite and wadsleyite in the deformed chondrule are confined to the former porphyritic olivine crystals. They display a spatially concentric arrangement: wadsleyite in the cores of the former olivines and ringwoodite surrounding it. Olivine–wadsleyite, olivine–ringwoodite, and wadsleyite–ringwoodite assemblages were found in several shocked chondrites and were produced in high-pressure synthetic samples. The transformation mechanisms of these phases have been regarded so far as a solid-state transformation. When large single olivine crystals are transformed to wadsleyite or ringwoodite under high-pressure and -temperature conditions, transformations of olivine are followed by the grain boundary or presumably intracrystalline nucleation-growth mechanisms (2, 17–19). The transformation from ringwoodite to wadsleyite is followed by a shear mechanism, whereas that from wadsleyite to ringwoodite is followed by a grain boundary nucleation-growth mechanism (20, 21). At any case, both mechanisms lead to high-pressure polymorphs not different in composition from parental olivine. In the case of the shock-melt vein of Peace River L6 chondrite, the spatial arrangement of a dominant phase in the wadsleyite–ringwoodite assemblage was different for each polymorph between the core and the rim of the assemblage (i.e., wadsleyite crystallites dominate in the core part, whereas ringwoodite crystallites dominate in the rim) (Fig. 1 *a–c*). There is
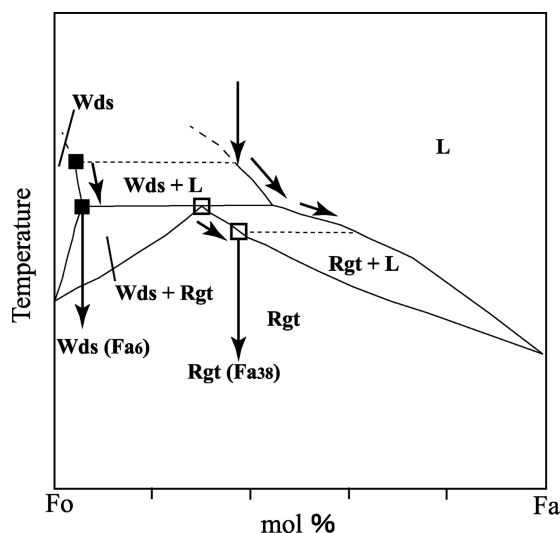
Table 1. Average chemical compositions of ringwoodite and wadsleyite

	Slice no. 1				Slice no. 3							
	Rgt		Wds		Rgt		Wds		Dendrite part		Core part	
Oxide	(11)	σ	(6)	σ	(8)	σ	(7)	σ	(7)	σ	(6)	σ
SiO_2	38.1	1.1	41.5	0.9	37.5	0.5	39.5	1.6	36.1	1.9	39.6	0.8
FeO	29.8	1.7	9.0	0.6	26.9	0.8	8.3	2.3	24.6	6.5	18.0	0.6
MgO	32.0	1.4	49.3	1.1	35.6	1.2	52.1	1.7	39.4	5.9	42.4	1.2
Total (wt %)	100		100		100		100		100		100	
Formula (O = 4)												
Si	1.02		1.01		1.00		0.97				1.01	
Fe(II)	0.67		0.18		0.60		0.17				0.38	
Mg	1.28		1.79		1.41		1.90				1.61	
Mg#	66		91		70		92		74		81	

All iron is assumed ferrous. Analyses are normalized to 100%. The chemical compositions were determined by using theoretical k factors. The numbers of analyses performed are in parentheses. Rgt, ringwoodite; Wds, wadsleyite. Mg# = $100 \times Mg/(Mg + Fe^{2+})$.

obvious enrichment or depletion in Mg and Fe contents between ringwoodite and wadsleyite, respectively (Table 1). Such wadsleyite–ringwoodite assemblage was also identified in a shock-melt vein of ALH78003, although the core part seems to be occupied by ringwoodite and the rim consists of wadsleyite crystallites (12). The ringwoodite core was enriched in FeO with MgO/(MgO + FeO) ≈ 0.74, whereas the wadsleyite rim was enriched in MgO with MgO/(MgO + FeO) ≈ 0.83. It was considered that the enrichment of and depletion in Mg and Fe might have been induced by Mg–Fe interdiffusion. The validity of such a mechanism could be tested by calculating the pertinent duration by using experimentally determined interdiffusion parameters. The duration of heating and pressure required for the Mg–Fe interdiffusion could then be estimated by using the Mg–Fe interdiffusion coefficients in wadsleyite experimentally determined previously (22, 23). However, the resultant estimates unambiguously show that it is impossible to explain the enrichment and depletion of Mg and Fe in ringwoodite and wadsleyite, respectively, in ALH78003 by Mg–Fe solid-state interdiffusion because anomalous long and unrealistic durations (50–500 s) of a shock event were necessary for the Mg–Fe interdiffusion (12). Similarly, there is obvious larger enrichment of and depletion in Mg–Fe between ringwoodite with MgO/(MgO + FeO) ≈ 0.60 and wadsleyite with MgO/(MgO + FeO) ≈ 0.89 in the former olivines in the squeezed chondrule entrained in the shock-melt vein of Peace River L6 chondrite. It is considered that wadsleyite and ringwoodite were not formed by solid-state interdiffusion under the equilibrium conditions, which is demonstrated by the phase diagram for the system Mg_2SiO_4–Fe_2SiO_4 (Fig. 4).

The deformed chondrule might have been partially melted because it was squeezed and flattened, implying strong plastic deformation. The formations of the high-pressure polymorphs (e.g., majorite-pyrope$_{ss}$ and magnesiowüstite from melts induced by a shock event) have been proposed by several authors (1, 25). Not every mineral in the deformed chondrule retained its original shape. We also see evidence for melting of FeNi metal, melting of only few plagioclase but no melting of the Ca-poor pyroxene in the chondrule matrix. We envisage that the reason only olivine and metal (and few plagioclase) were melted would be due to a difference in shock impedance between them and the Ca-poor pyroxene, along with shear stress and the high thermal stress. We envisage from the concentric wadsleyite–ringwoodite texture and their contrasting chemical compositions that both ringwoodite and wadsleyite fractionally crystallized from an olivine melt alone. The temperature during the shock event would then be 1,700–1,900°C because the whole deformed chondrule would not be heated beyond the liquidus line (15). Fig. 5 schematically

depicts a phase diagram interpreting the formation process of the ringwoodite–wadsleyite assemblage. Although a melting experiment of ringwoodite has not been conducted yet, the phase diagram can be estimated based on the melting experiments of olivine (26). Accordingly, original olivine was melted by a shock wave induced by an impact. First, wadsleyite with high Mg# fractionally crystallized (wadsleyite core formation) from the melt ($Fa_{24–26}$ of the original unzoned olivines). Subsequently, ringwoodite with low Mg# was formed from the melt depleted in Mg around the wadsleyite core (ringwoodite rim formation) during a decreasing of temperature, but still at high pressure. The chemical composition of the wadsleyite

Fig. 4. Pressure-composition diagram for the Mg_2SiO_4(Fo)–Fe_2SiO_4(Fa) system at 1,200°C (24). Chemical compositions (in mol % fayalite) of wadsleyite and ringwoodite in the olivine porphyritic chondrule in the Peace River L6 chondrite are indicated by a red bar and a blue bar, respectively. The original composition of the individual olivines is indicated by a green bar. Rgt, ringwoodite; Wds, wadsleyite; Pv, perovskite; Mg-wü, magnesiowüstite; Sti, stishovite.

GEOLOGY

Fig. 5. A simplified schematic diagram interpreting the path of wadsleyite–ringwoodite fractional crystallization from the olivine melt.

core was fixed because it was covered with the growing ringwoodite rim and could not react with the melt any more. Ringwoodite with low Mg# continued to form from the residual melt depleted in Mg. We argue that the dendrite-like texture (Fig. 3*b*) supports our interpretation. The core part of the dendrite-like texture is wadsleyite that first crystallized from the molten olivine. The wadsleyite and residual liquid are retained through quenching. The wadsleyite (Fa$_{19}$) in the core of the dendrite-like intergrowth is depleted in Mg, compared with other wadsleyite crystallites (Fa$_9$), because the former crystallized in the final stages from an olivine melt already depleted in Mg during quenching and solidification.

The compositions of ringwoodite and wadsleyite crystallites in the "granoblastic-like" assemblage (Fig. 2*b*) are indicative of disequilibrium because the different crystallites did not *in situ* crystallize together from the melt in this intergrowth, but represent crystallites fragmented from their parental regions and fortuitously reassembled together just before solidification and quenching. The crystallization of the wadsleyite–ringwoodite assemblage originally proceeded from core to rim. Deformation and accompanied shear stress involved during squeezing of the wadsleyite–ringwoodite mesh in the individual olivine melts could induce the spatial separation of the dense polymorphs, followed by contemporaneous fragmentation of the two spatially separated polymorph regions to multiple mixed crystallites. This deformation induced the observed stacking faults in ringwoodite and wadsleyite. We emphasize that the assemblage and its texture present in every individual olivine melt pocket depicts a frozen step of the above-inferred stages depending on the thermal stress to which every individual olivine was subjected as a result of its distance from the hot melt vein, but at the same total pressure in vein and individual objects entrained in.

Open fractures occur within and around the ringwoodite–wadsleyite assemblages (Figs. 1–3). The fractures could have formed after decompression by volume decrease after crystallization of ringwoodite and wadsleyite. If original olivine and its high-pressure polymorphs, wadsleyite and ringwoodite, have the same Mg#, the olivine–wadsleyite transformation needs 3.16–3.20 cm^3/mol, whereas the olivine–ringwoodite transformation requires a 4.14–4.24 cm^3/mol difference (27). Some of these open fractures were filled with iron-nickel metal liquid, which was later oxidized by terrestrial weathering after

cooling and solidification. Iron or iron-nickel metal in the matrix of the shock-melt vein, which partly melted, was mobilized into the open fractures. At any case, the growth textures of wadsleyite and ringwoodite, their contrasting chemistries, and the dendritic quench-type texture around wadsleyite grains are stark evidence for the fractional crystallization of both minerals from a liquid of olivine composition. This interpretation erases the conundrum resulting from the assumption of formation by solid-state phase transformation and solely applying EPMA (electron probe micro analysis) techniques alone, giving average compositions of mixed crystallites of different phases altogether smaller in volume than the electron beam volume and uncritical TEM investigations (10) that lead to unrealistic time scales. In comparison, measurements of compositional profiles in nanometer steps using nanosecondary ionization mass spectrometry revealed unambiguous time scales (11).

Materials and Methods

We studied several polished thin sections of shock-melt veins in Peace River chondrite. Entrained in the veins are many large olivine, Ca-poor pyroxene grains and few olivine, porphyritic chondrules. Chondrules and minerals were optically investigated in reflected light and with a field emission scanning electron microscope in a back-scattered-electron (BSE) mode. Chemical compositions of the minerals of interest were conducted with a JEOL electron microprobe at the Bayerische Geoinstitut in Bayreuth at 15 keV operating voltage and 20 nA sample current. Microprobe standards used included olivine and orthopyroxene, with well known compositions for Fe, Mg, Mn, and Si.

The natures of the minerals under investigations were determined by using the laser microRaman facility of the Ecole Normale Supérieur de Lyon at the following conditions. To check the mineral phases and to clarify the relationship between olivine and its high-pressure polymorphs, individual Raman measurements and mapping were performed. Unpolarized Raman spectra were collected with Jobin Yvon LabRam HR800 microspectrometers. The Raman device was composed of an argon ion laser tuned at 514.5 nm, gratings of 1,800 g/mm, and a visible CCD camera. The spectrometer was used in backscattering geometry. The laser beam was focused through microscope objectives (magnification ×100) down to a 1-μm spot on the sample, and the backscattered light was collected through the same objective. Acquisition times were typically 300 s. The laser power on the sample was kept at 50 mW to avoid any damage. For each phase, two spectra were acquired in the spectral region of 200–1,500 cm^{-1} and averaged afterward. Further investigation of the relationship between the different phases was conducted by using Raman mapping. Raman maps were acquired with a motorized XY stage. A high resolution was reached with steps of submicrometric stage movements. Each spot was measured for 3 s, and two spectra were collected in the spectral range of 100–1,900 cm^{-1} and averaged afterward. The spot size is 1 μm, and this same size was used as a step for the mapping. Each phase was identified by using their main band (the 855-cm^{-1} peak for olivine, the 917-cm^{-1} band for wadsleyite, the 794-cm^{-1} peak for ringwoodite, and the 1,000-cm^{-1} band for pyroxene). The color scale on the map is calculated from the integrated band intensity.

The flattened and squeezed chondrule containing both ringwoodite and wadsleyite was cored out for TEM by using a high-precision microdrill. The grain investigated originally consisted of two olivine crystals. A TEM foil of a target area to be studied by TEM was prepared by a FIB system. A JEOL JEM-9320 FIB and a dedicated optical microscope with a manipulator were used to recover the targeted cut foil within the grain. A gallium ion beam was accelerated to 30 kV during the sputtering of the specimen by FIB. The resultant TEM foil was 120–130 nm in thickness. A detailed FIB procedure is described in ref. 28. A JEOL JEM-2010 TEM operating at 200 kV was used for conventional TEM (CTEM) and SAED. We also used an STEM, a JEOL JEM-3000F field emission TEM operating at 300 kV with a JEOL EDS detector system. EDS elemental mapping and quantitative analysis were performed by using a JEOL JEM-3000F. Elemental mapping images were taken by using emitted x-ray distribution maps of Mg–Kα, Al–Kα, Si–Kα, and Fe–Kα lines. The pixel size of each image was 256 × 256. The correcting time was limited to 0.5 ms at one point to prevent electron damage during mapping. The beam-drift correction was implemented after scanning one or two areas. The chemical compositions were determined by using theoretical *k* factors (29).

1. Chen M, *et al*. (1996) The majorite-pyrope + magnesiowüstite assemblage: Constrains on the history of shock veins in chondrites. *Science* 271:1570–1573.
2. Kerschhofer L, *et al*. (2000) Kinetics of intracrystalline olivine–ringwoodite transformation. *Phys Earth Planet Inter* 121:59–76.
3. Mosenfelder JL, *et al*. (2001) Experimental constrains on the depth of olivine metastability in subducting lithosphere. *Phys Earth Planet Inter* 127:165–180.
4. Putnis A, Price GD (1979) High-pressure (Mg, Fe)$_2$SiO$_4$ phases in the Tenham chondritic meteorite. *Nature* 280:217–218.
5. Ohtani E, *et al*. (2004) Formation of high-pressure minerals in shocked L6 chondrite Yamato 791384: Constrains on shock conditions and parent body size. *Earth Planet Sci Lett* 227:505–515.
6. Price GD, Putnis A, Agrell SO (1979) Electron petrography of shocked-produced veins in the Tenham chondrite. *Contrib Miner Petrol* 71:211–218.
7. Madon M, Poirier J-P (1980) Dislocations in spinel and garnet high-pressure polymorphs of olivine and pyroxene: Implications for mantle rheology. *Science* 207:66–68.
8. Chen M, El Goresy A, Gillet P (2004) Ringwoodite lamellae in olivine: Clue to olivine–ringwoodite phase transition mechanisms in shocked meteorites and subducting slabs. *Proc Natl Acad Sci USA* 101:15033–15037.
9. Chen M, *et al*. (2006) Fracture-related intracrystalline transformation of olivine to ringwoodite in the shocked Sixiangkou meteorite. *Meteorit Planet Sci* 41:731–737.
10. Chen M, Chen J, Xie X, Xu J (2007) A microstructural investigation of natural lamellar ringwoodite in olivine of the shocked Sixiangkou chondrite. *Earth Planet Sci Lett* 264:277–283.
11. Beck P, Gillet Ph, El Goresy A, Mostefaoui S (2005) Timescales of shock processes in chondritic and martian meteorites. *Nature* 435:1071–1074.
12. Ohtani E, *et al*. (2006) High-pressure minerals in shocked L6-chondrites: Constrains on impact conditions. *Shock Waves* 16:45–52.
13. Price GD, Putnis A, Smith DGW (1982) A spinel to β-phase transformation mechanism in (Mg, Fe)$_2$SiO$_4$. *Nature* 296:729–731.
14. Price GD (1983) The nature and significance of stacking faults in wadsleyite, natural β-(Mg, Fe)$_2$SiO$_4$ from the Peace River meteorite. *Phys Earth Planet Inter* 33:137–147.
15. Agee CB, Li J, Shannon MC, Circone S (1995) Pressure-temperature phase diagram for the Allende meteorite. *J Geophys Res* 100:17725–17740.
16. Asahara Y, Kubo T, Kondo T (2004) Phase relations of a carbonaceous chondrite at lower mantle condition. *Phys Earth Planet Inter* 143–144:421–432.
17. Kerschhofer L, Sharp TG, Rubie DC (1996) Intracrystalline transformation of olivine to wadsleyite and ringwoodite under subduction zone conditions. *Science* 274:79–81.
18. Kerschhofer L, *et al*. (1998) Polymorphic transformations between olivine, wadsleyite and ringwoodite: Mechanisms of intracrystalline nucleation and the role of elastic strain. *Phys Earth Planet Inter* 101:15033–15037.
19. Kubo T, Ohtani E, Funakoshi K (2004) Nucleation and growth kinetics of the α–β transformation in Mg$_2$SiO$_4$ determined by *in situ* synchrotron powder X-ray diffraction. *Am Miner* 89:285–293.
20. Rubie DC, Brearley AJ (1990) Mechanism of the α–β phase transformation of Mg$_2$SiO$_4$ at high temperature and pressure. *Nature* 348:628–631.
21. Rubie DC, Brearley AJ (1994) Phase transitions between and (Mg, Fe)$_2$SiO$_4$ in the Earth's mantle: Mechanisms and rheological implications. *Science* 264:1445–1448.
22. Chakraborty S, *et al*. (1999) Enhancement of cation diffusion rates across the 410-kilometer discontinuity in Earth's mantle. *Science* 283:362–365.
23. Kubo T, Shimojuku A, Ohtani E (2004) Mg-Fe interdiffusion rates in wadsleyite and the diffusivity jump at the 410-km discontinuity. *Phys Chem Miner* 31:456–464.
24. Agee CB (1999) Phase transformations and seismic structure in the upper mantle and transition zone. *Rev Mineral* 37:165–203.
25. Langenhorst F, Poirier J-P (2000) Anatomy of black veins in Zagami: Clues to the formation of high-pressure phases. *Earth Planet Sci Lett* 184:37–55.
26. Ohtani E, Moriwaki K, Kato T, Onuma K (1998) Melting and crystal–liquid partitioning in the system Mg$_2$SiO$_4$-Fe$_2$SiO$_4$ to 25 GPa. *Phys Earth Planet Inter* 107:75–82.
27. Akaogi M, Ito E, Navrotsky A (1989) Olivine-modified spinel–spinel transitions in the system Mg$_2$SiO$_4$-Fe$_2$SiO$_4$: Calorimetric measurements, thermochemical calculation and geophysical application. *J Geophys Res* 94:15671–15685.
28. Miyahara M, *et al*. (2008) Application of FIB system to ultra-high-pressure Earth science. *J Miner Petrol Sci* 103:88–93.
29. Cliff G, Lorimer GW (1975) The quantitative analysis of thin specimens. *J Microscopy* 103:203–207.

GEOLOGY